catalysts

MDPI

Article

Co_3O_4 Nanoparticle-Decorated N-Doped Mesoporous Carbon Nanofibers as an Efficient Catalyst for Oxygen Reduction Reaction

Hairong Xue [1,2], Tao Wang [1,*], Hao Gong [1], Hu Guo [1], Xiaoli Fan [1], Li Song [1], Wei Xia [1], Yaya Feng [1] and Jianping He [1,*]

[1] College of Materials Science and Technology, Jiangsu Key Laboratory of Materials and Technology for Energy Conversion, Nanjing University of Aeronautics and Astronautics, Nanjing 210016, China; xuehairong@zjut.edu.cn (H.X.); gonghao@nuaa.edu.cn (H.G.); guohu21@nuaa.edu.cn (H.G.); Fan_xiaoli@nuaa.edu.cn (X.F.); songli@nuaa.edu.cn (L.S.); xiaweifriend@163.com (W.X.); nuaafengyaya@nuaa.edu.cn (Y.F.)

[2] College of Chemical Engineering, Zhejiang University of Technology, Hangzhou 310014, China

* Correspondence: wangtao0729@nuaa.edu.cn (T.W.); jianph@nuaa.edu.cn (J.H.); Tel.: +86-25-5211-2906 (T.W. & J.H.)

Academic Editors: Adam F. Lee, Jean-Philippe Dacquin and Karen Wilson
Received: 20 April 2017; Accepted: 9 June 2017; Published: 15 June 2017

Abstract: A low cost, durable, and efficient electrocatalyst for oxygen reduction reactions (ORR) is essential for high-performance fuel cells. Here, we fabricated Co_3O_4 nanoparticles (NPs) anchored on N-doped mesoporous carbon nanofibers (Co_3O_4/NMCF) by electrospinning combined with the simple heat treatment. Within this composite, carbon nanofibers possess a mesoporous structure, contributed to obtain a high surface area, which can facilitate the infiltration of electrolyte. Moreover, this one-dimensional (1D) carbon nanofiber also acts as a 1D conductive channel, effectively improving the transmission of electrons. In addition, the doping of the N element with high content combined with homogenously distributed Co_3O_4 NPs can significantly enhance the ORR electrocatalytic activity. Benefiting from the advantages of material and structure, the Co_3O_4/NMCF catalyst favors a four electron transfer process in alkaline media, exhibiting good ORR electrocatalytic activity, and its durability is much better than that of commercial Pt/C.

Keywords: Co_3O_4 nanoparticles; N-doped mesoporous carbon nanfiber; electrospinning; electrocatalyst; oxygen reduction reaction; fuel cell

1. Introduction

In order to meet the requirements of the global energy demand, fuel cells (FCs) are a promising choice for the clean and sustainable energy storage and conversion devices, profiting from their high energy density, low cost, long cycle life, and safety [1,2]. However, the catalyst, especially for oxygen reduction reactions (ORR), has been a technological bottleneck for the large-scale commercialization of FCs [3,4]. Traditionally, Pt-based materials have been the most widely used as typical catalysts for ORR in FCs. However, high cost, poor durability, sluggish oxygen reduction, and carbon monoxide (CO) poisoning have limited Pt-based catalysts to expand their commercial application [2]. Consequently, intensive research efforts are aimed at developing nonprecious metal-based electrocatalysts to replace Pt-based catalysts [5,6]. To date, transition metal oxide-based (TMOs) materials have attracted more attention of researchers, because of their respectable ORR catalytic activity, low cost, and high catalytic durability [7–14].

Of the various TMOs materials, cobalt-based TMOs with high cost effective have been considered as a promising alternative candidate for Pt-based catalysts [9–14]. Unfortunately, pure cobalt-based TMOs—the same as other TMOs—are semiconductors, so poor electrical conductivity limits their catalytic performance. In order to meet the requirement for commercial application in FCs, it is necessary to further explore some efficient strategies to improve the catalytic performance of the pure cobalt-based TMOs. Recently, cobalt-based TMOs nanoparticle (NP) decorated N-doped carbon materials were found to exhibit excellent ORR catalytic performance [9,10,13,14]. Chen et al. [10] constructed CoO nanoparticles decorated 3D crumpled nitrogen-doped graphene (CG) hybrid material through an aerosolization method. In an alkaline electrolyte, the ORR catalytic activity of CG-CoO catalyst is comparable with that of the commercial Pt/C and its durability is much better than of the Pt/C. Dai et al. [13] reported a Co_3O_4/N-doped reduced graphene oxide (N-G) hybrid material prepared by using a simple two-step method, which exhibits high catalytic activity for ORR. They also synthesized CoO/nitrogen-doped carbon nanotube (N-CNT) composite, in which the CoO nanocrystals are directly grown on oxidized CNTs. This high-performance catalyst with the four-electron reduction pathway shows high ORR current density, which outperformed commercial Pt/C catalyst [14]. Therefore, the fabrication of cobalt-based TMOs NP-decorated N-doped carbon catalysts appears to be an effective approach to obtain ORR catalysts with high catalytic performance.

Despite the above promising results, the practical application of the cobalt-based TMOs NP-decorated N-CNT or N-G is still hindered by several key problems. Both N-CNT and N-G are confronted with numerous difficulties, such as high cost, low yield, and sophisticated fabrication. Thus, it is necessary to develop low cost, simple, and scalable strategies to design and synthesize cobalt-based TMOs NP-decorated N-doped carbon catalysts with excellent ORR catalytic performance for practical applications. Because of their high electrochemical stability and good electrical conductivity, unique one-dimensional (1D) porous carbon nanofibers (CNFs) have received considerable attention [15–17]. More importantly, the inexpensive CNFs have high specific surface area and various controlled structures in comparison to CNTs. Hence, we report a facile method of Co_3O_4 NP-decorated N-doped mesoporous carbon nanofibers (Co_3O_4@NMCF) by using electrospinning combined with thermal treatment. As a result, the high content N element (~6.51 At. %) was successfully doped into the mesoporous carbon nanofibers (MCFs) and existed in the form of pyridine- and quaternary-N. Moreover, Co_3O_4 NPs uniformly disperse in the 1D MCFs. Benefiting from enhanced surface properties, optimized porous structure, perfect 1D conductive channel of NMCFs, and high catalytic activity of Co_3O_4 NPs, the as-prepared Co_3O_4@NMCF catalyst possesses good ORR catalytic activity in alkaline aqueous electrolyte.

2. Results and Discussion

The fabrication process of Co_3O_4@NMCF composite is shown in Figure 1, which was prepared by electrospinning combined with multi-step heat treatment. After electrospinning, the obtained polymer hybrid nanofibers further underwent pre-oxidation in air to achieve good thermal stabilization. During carbonization in N_2 atmosphere at 800 °C, the Co salt precursor was decomposed and then reduced to metal Co due to the carbothermic reduction. Finally, the metal Co NPs were converted to Co_3O_4 NPs by reoxidation in air, anchored on the N-doped carbon nanofibers. In this work, both PAN and PVP serve as carbon and nitrogen sources. After stirring for a long time, PVP can coordinate with Co^{2+} well due to its lactam groups, which is beneficial to form a uniformly PVP/$Co(Ac)_2$ solution. Figure S1 illustrates the above mechanism. Benefiting from the different viscosities of the polymers, the PAN, PVP, and $Co(Ac)_2$ can be separated into PAN (discontinuous phases) and PVP/$Co(Ac)_2$ (continuous phases) solution. Therefore, the Co_3O_4 NPs can easily and uniformly anchor on the carbon nanofiber after the calcining treatment.

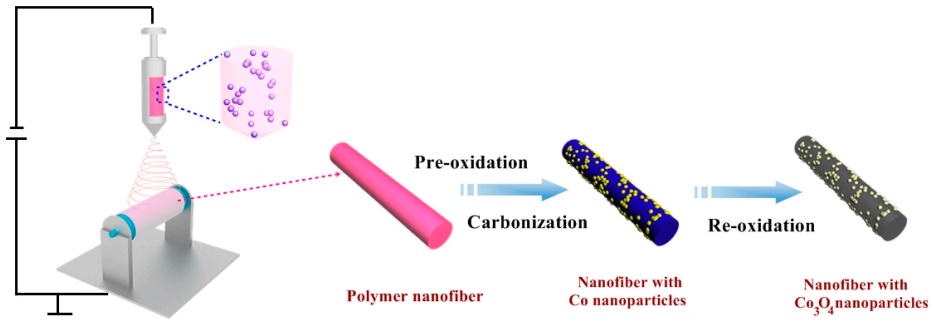

Figure 1. Schematic diagram for the fabrication of Co_3O_4@NMCF composite.

Figure 2a shows the X-ray diffraction (XRD) of Co_3O_4@NMCF composite. All diffraction peaks match well with the spinel structure of Co_3O_4 crystalline (JCPDS card no. 43-1003). As is shown in Figure 2b, X-ray photoelectron spectrum shows that four elements (Co, O, N, and C) distribute within the Co_3O_4 NP-decorated N-doped mesoporous carbon nanofibers, indicating successful synthesis of the composite. Moreover, it can be found that carbon nanofibers possess a certain extent graphitization, evidenced by an obvious diffraction peak at around $2\theta = 26^\circ$ indexed to the (002) crystallographic plane of carbon. Normally, Raman spectroscopic measurement (Figure S2) can be used to determine graphitization degree of carbon materials. For the graphitic carbon, its graphitic structure can be reflected by the I_D/I_G ratio, because the number of its defect sites is proportional to the I_D/I_G ratio. So, if the I_D/I_G is higher, the graphitization degree is lower. Based on the Raman results, we found that NMCF shown a certain extent graphitization, evidenced by the relatively low ratio of I_D/I_G (~1.0). This result can be further verified by the C1s spectrum. As shown in Figure 2c, the deconvoluted four peaks of the C1s spectrum at 284.7, 286.4, and 288.5 eV are associated with the pure graphitic sites; C–O and C=O bond, respectively, of which the pure graphitic sites make up most of the C1s spectrum [18–21]. Figure 2d shows the Co2p spectrum, which can further confirm the valence state of elements and detailed composition of Co_3O_4. The Co2p spectrum is well fitted with one shakeup satellite and two spin-orbit doublets, ascribed to Co^{2+} and Co^{3+} [11,12,22,23]. More importantly, the two main types of N element are further revealed by the N1s spectrum (Figure 2e), including quaternary-N and pyridinic-N [24–26]. Due to the decomposition of poly(vinylpyrrolidone) (PVP) and polyacrylonitrile (PAN), the N element can be successfully doped into the carbon nanofiber. The nitrogen doping content of NMCF is 6.51 At. %, which is calculated from N1s spectrum. The total mass loading of the Co_3O_4 is ~11.1 wt %, calculated by the TG analysis (Figure 2f).

Figure 3a shows the FESEM image of the polymer hybrid nanofibers, which possess the one-dimensional nanofiber structure, uniform diameter (~500 nm) and smooth surfaces. As compared to the precursors, the Co_3O_4@NMCF composite retains the 1D structure but has a smaller diameter (~250 nm) after multi-step heat treatment, shown in Figure 3b. Furthermore, the numerous Co_3O_4 NPs are uniformly anchored on the nanofiber surface. It can be observed that the particle size of the Co_3O_4 NPs ranges from 20 to 100 nm, evidenced by the TEM and HRTEM images (Figure 3c,d). Moreover, as shown in Figure 3e, there is an interplanar spacing (0.201 nm) in the Co_3O_4 NP, corresponding to the spinel (400) plane, which suggests a high crystallinity of Co_3O_4 NPs. In addition, the N_2 adsorption/desorption isotherms of Co_3O_4@NMCF composite and its corresponding pore-size distribution curves are illustrated in Figure 3f. As shown in Figure 3f, type-IV curves with an H1-type hysteresis loop are presented in N_2 adsorption/desorption isotherms of the sample, suggesting that Co_3O_4@NMCF composite has a typical mesoporous structure [27,28]. The pore-size distribution curves (inset of Figure 3f) show a narrow pore-size distribution, centered at ~5 nm. Based on the BET methods, the specific surface area the Co_3O_4@NMCF composite are close to 370 $m^2\ g^{-1}$, and its pore-size is 5.1 nm estimated by BJH model, which further confirm its mesoporous structure.

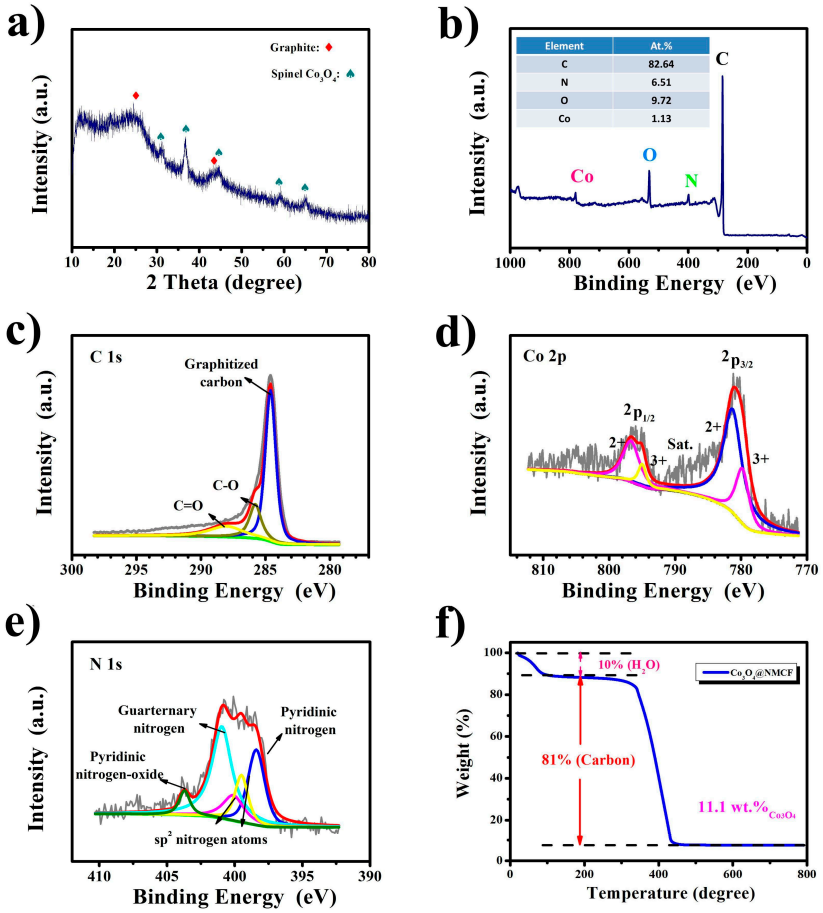

Figure 2. (**a**) XRD patterns, (**b**–**e**) X-ray photoelectron spectrum, (**f**) TG curve of the Co_3O_4@NMCF composite; The table (inset of (**b**)) summarizes the elemental composition for Co_3O_4@NMCF obtained from XPS measurement.

The cyclic voltammetry (CV) curves of Co_3O_4@NMCF and commercial Pt/C (20%) catalysts are shown in Figure 4a shows, tested in N_2 or O_2-saturated KOH solution (0.1 M). Due to the presence of O_2, the two catalysts all exhibited an obvious cathodic peak, which indicate a substantial ORR process. As observed, the onset potential (E_{onset}) and reduction peak potential (E_{peak}) for the ORR of Co_3O_4@NMCF catalyst is similar to that of the commercial Pt/C (20%) catalyst. As shown in Figure 4b, the linear sweep voltammetry (LSV) curves of Co_3O_4@NMCF catalyst show that its limiting current density (JL) and E_{onset} are closed to that of the Pt/C (20%) catalyst, suggesting the high ORR catalytic activity of Co_3O_4@NMCF catalyst. In addition, the rotating ring-disk electrode (RRDE) measurements were used to analyze the ORR mechanism of Co_3O_4@NMCF catalyst, conducted in O_2-saturated KOH solution (0.1 M). For the Co_3O_4@NMCF catalyst, its ring current (i_r) (the oxidation of HO_2^-) is much smaller than the disk current (i_d) and even negligible, suggesting that the HO_2^- evolution is prominently suppressed in the ORR process. Based on the ring and disk current, the HO_2^- yield and electron transfer number (n) of Co_3O_4@NMCF and Pt/C (20%) catalysts can be calculated, shown in Figure 4c. Over the scanning potential range, the HO_2^- yield of Co_3O_4@NMCF catalyst is below 7%, and its corresponding n is almost constant and close to 4 from −0.2 to −0.8 V during the reaction. Compared with the RRDE results of Pt/C (20%), the low HO_2^- yield and high n indicate a near four electron reaction dominant pathway. Moreover, Tafel plots of Co_3O_4@NMCF and Pt/C (20%) catalysts derived from the LSV curves (Figure 4b) were shown in Figure 4d, which can further examine their ORR kinetics. The Tafel slope of Co_3O_4@NMCF catalyst (48 mV dec^{-1}) at low potentials is smaller than that of Pt/C (20%) (96 mV dec^{-1}), suggesting the first electron transfer of the rate determining step.

The chronoamperometric measurement was performed at −0.3 V (vs. SCE) to evaluate the durability of the ORR catalytic activity for the two catalysts. It can be seen in Figure 4e, after 3600 s of testing, that the initial activity of Co_3O_4@NMCF catalyst decreases only 6.2%, while Pt/C (20%) catalyst shows the increased initial activity decay (14.2%), indicating that Co_3O_4@NMCF catalyst possesses much higher stability. In order to evaluate the role of Co_3O_4 NPs in ORR, we also have prepared NMCF sample without Co_3O_4, which can be confirmed by the TEM images (Figure S3a,b) in and XRD (Figure S3c). Based on the result of LSV test (Figure S3d), Co_3O_4@NMCF catalyst shows the much better ORR catalytic activity than NMCF catalyst in alkaline conditions, indicating that the Co_3O_4 NPs plays much significant role in ORR. The above results indicate that Co_3O_4@NMCF catalyst shows the high ORR catalytic activity and the remarkable stability, which can be served as a highly efficient ORR electrocatalyst. The superior ORR catalytic activity of the Co_3O_4@NMCF catalyst mainly benefits from the material and structural advantages. Figure 4f shows the ORR catalytic mechanism of the Co_3O_4@NMCF catalyst. The Co_3O_4 NPs have the high ORR catalytic activity, uniformly anchored on the N-doped carbon nanofibers, which can provide a lot of catalytic active sites for ORR due to the efficient contact with O_2 and electrolyte. Moreover, the 1D carbon nanofibers directly serve as a conductive channel to ensure the fast electron transport. Furthermore, the mesoporous structure of carbon nanofibers is not only beneficial for obtaining high specific surface area, but also can facilitate O_2 diffusion and electrolyte infiltration. In addition, the carbon nanofiber has high N element content existed in the quaternary-N and pyridinic-N types. The doped N element in the carbon frameworks can cause the unique electronic properties due to the synergistic effect between N atom (lone electron pairs) and the graphite (π-conjugated system). As an n-type dopant, the N atom doped into graphitized carbon can increase electric charge density, which is conducive to ORR process, thus improving the ORR catalytic activity. Due to the above-mentioned advantages of the Co_3O_4@NMCF composite architecture, the Co_3O_4@NMCF cathode achieved a remarkable electrocatalytic performance for ORR.

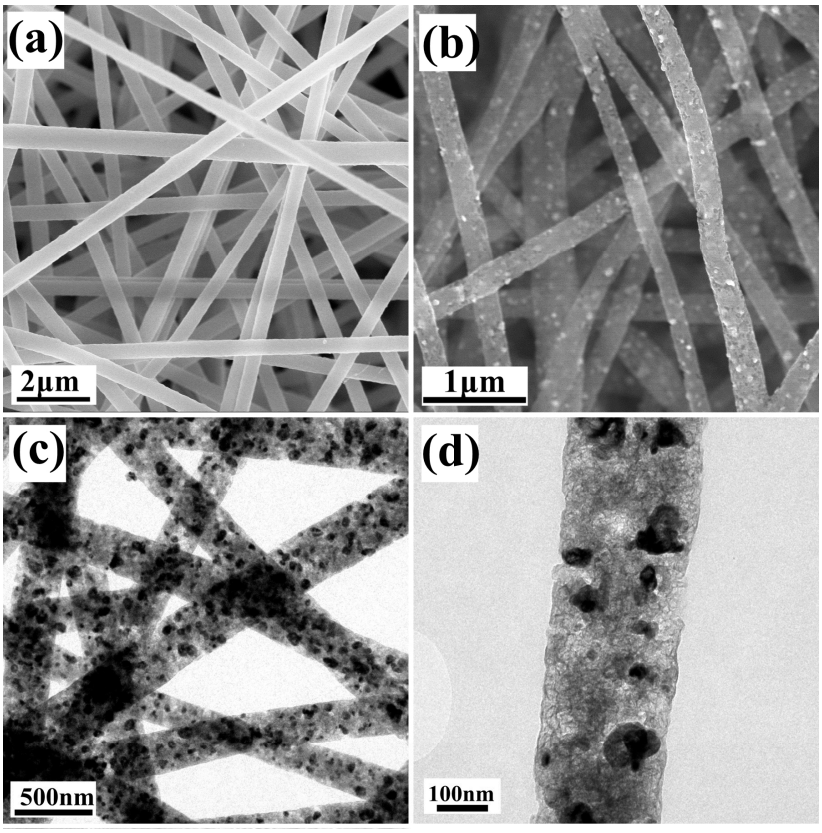

Figure 3. *Cont.*

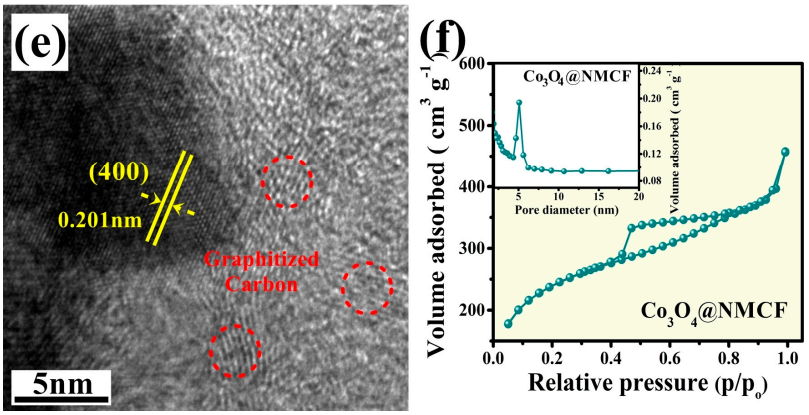

Figure 3. (**a**) SEM image of the polymer hybrid nanofibers; (**b**) SEM, (**c**,**d**) TEM, (**e**) HRTEM images; (**f**) N_2 adsorption/desorption isotherms and pore-size distribution curves (inset) of the Co_3O_4@NMCF composite.

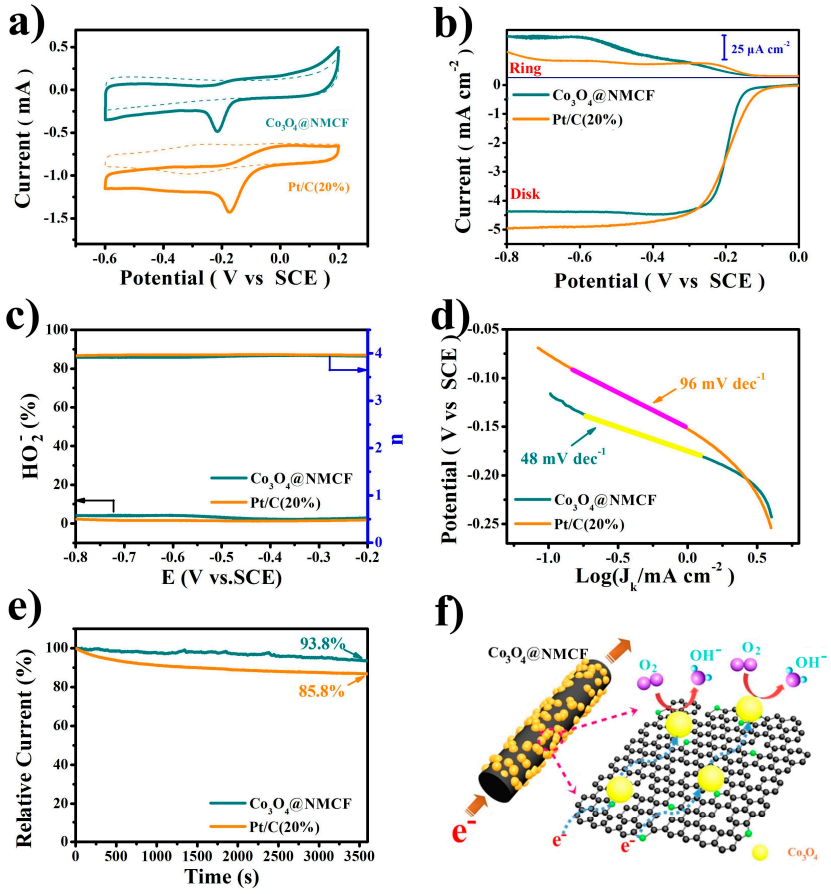

Figure 4. (**a**) CV curves (dash line: N_2; solid line: O_2), (**b**) RRDE voltammograms at 1600 rpm, (**c**) OH_2^- yield and corresponding electron transfer number, (**d**) the Tafel slope, (**e**) chronoamperometric responses of Co_3O_4@NMCF and commercial Pt/C catalysts; (**f**) The catalytic mechanism for ORR of the Co_3O_4@NMCF catalyst; the scanning rates of CV and RRDE tests are 20 and 5 mV s^{-1} respectively.

3. Materials and Methods

3.1. Fabrication of Co_3O_4 NP-Decorated N-Doped Mesoporous Carbon Nanofibers

The Co_3O_4 NP-decorated N-doped mesoporous carbon nanofibers (Co_3O_4@NMCFs) were synthesized by using an electrospinning technique combined with the subsequent multi-step heat treatments. Typically, the cobalt acetylacetonate ($Co(acac)_2$) (0.2 g) and PVP (0.5 g) were dissolved into the *N*,*N*-dimethylformamide (DMF) (5 mL) under vigorous stirring (50 °C, 2 h) to obtain the PVP solution. For PAN solution, the same as PVP solution, the PAN (0.5 g) was dissolved into DMF (5 mL) and then followed by vigorous stirring (80 °C, 1 h). Then, the above two solutions were mixed with vigorous stirring at 80 °C. The resultant hybrid solution was loaded into a syringe with a single needle of the diameter 0.5 mm. In this experiment, the distance between the collector (aluminum foil) and needle (12 cm), applied voltage (12 kV) and flow rate (0.1 mm min^{-1}) were adopted in the electrospinning process. After drying in the vacuum oven (70 °C, 24 h), the as-electrospun polymer film was used to heat for multi-step procedure. Details are as follows: the dried polymer film was firstly heated in air (250 °C, 1.5 h, air), then heated in N_2 (350 °C, 5 h, N_2), further heated (800 °C, 1 h, N_2), and finally annealed (300 °C, 20 min, air) by using the heating rates of 5 and 1 °C min^{-1} in air and N_2, respectively. The as-prepared Co_3O_4 NP-decorated N-doped carbon nanofibers film was denoted as Co_3O_4@NMCF.

3.2. Material Characterizations

For the samples, their crystal structure was investigated by X-ray diffraction (XRD) (D8 Advance, Bruker Company, Karlsruhe, Germany). X-ray photoelectron spectroscopy (XPS) analysis (PHI 5000 VersaProbe, Ulvac-Phi Company, Kanagawa, Japan) was used to characterize the chemical compositions. Thermogravimetric/Differential thermal analysis (TG/DTA) (TGA 7, Perkin Elmer Company, Waltham, MA, USA) was used to calculate the weight retention of Co_3O_4. The morphology and microstructures were observed by field-emission scanning electron microscope (FE-SEM) (S-4800, Hitachi Company, Tokyo, Japan), transmission electron microscopy (TEM) (Tecnai-20, FEI Company, Hillsboro, OR, USA) and high-resolution transmission electron microscopy (HR-TEM) (JEM-2100, JEOL Company, Tokyo, Japan), respectively. The Brunauer–Emmett–Teller (BET) method was used to analyze the surface area analysis tested on Micromeritics ASAP 2010 (Micromeritics ASAP 2010, Norcross Company, Norcross, GA, USA).

3.3. Electrochemical Measurement

The Co_3O_4@NMCF and commercial Pt/C (20%) catalyst electrodes with a thin-film (0.1256 cm^2) was prepared by dropwise loading the catalyst ethanol suspension (5 mg of Co_3O_4@NMCF or commercial Pt/C (20%) catalyst, 50 μL of Nafion ethanol solution (5 wt %) and 1 mL of ethanol) on the GC electrode (4 mm in diameter) and then drying. The as-prepared catalyst loading was 625 μg cm^{-2}, and the commercial Pt/C (20%) was tested with Pt loading of 25 μg cm^{-2}. The electrochemical measurements were tested by using an electrochemical workstation (CH Instruments 660C, Chenhua Company, Shanghai, China), including cyclic voltammetry (CV) and rotating ring-disk electrode (RRDE). For RRDE electrode, its collection efficiency is 37%, the inner and outer diameters of ring electrode (GC) are 6.92 and 7.92 mm, and the diameter of disk electrode (Pt) is 5.61 mm. A typical three-electrode system was adopted, consisted of the Co_3O_4@NMCF catalyst electrode (working electrode), saturated calomel electrode (SCE) (reference electrode), and Pt foil electrode (counter electrode), respectively. The scan rates of RDE and CV experiments were 5 and 20 mV s^{-1}, respectively, tested in the O_2-saturated KOH solution (0.1 M).

4. Conclusions

In summary, the Co_3O_4 NPs uniformly anchored on the N-doped mesoporous carbon nanofiber (Co_3O_4/NMCF) has been successfully prepared by electrospinning combined with thermal treatment.

Its mesoporous structure offers high specific surface area, which is beneficial to facilitate the infiltration of electrolyte; the favorable conductive channel of 1D carbon nanofiber is conducive to the fast transfer of electrons. In addition, the homogenously distributed Co_3O_4 NPs and doping of the N element provide high catalytic activities for ORR. Therefore, the Co_3O_4/NMCF catalyst favors a four-electron transfer process and exhibits good electrochemical property. Moreover, its durability is much better than the commercial Pt/C catalyst during the ORR. Because of its superior electrochemical performance, Co_3O_4/NMCF composite is a promising choice, serving as an efficient electrocatalyst for ORR.

Supplementary Materials: The following are available online at www.mdpi.com/2073-4344/7/6/189/s1.

Acknowledgments: The authors express their appreciations for the financial support from the Natural Science Foundation of Jiangsu Province (BK20160795), the National Natural Science Foundation of China (51372115, 51602153 and 11575084), the Research Start-Up Fund of NUAA (90YAH16008), and a project funded by the Priority Academic Program Development of Jiangsu Higher Education Institutions (PAPD).

Author Contributions: Hairong Xue wrote the paper; Hairong Xue, Tao Wang, and Jianping He designed the experiments; Hairong Xue done the experiments; Hao Gong, Hu Guo, and Xiaoli Fan analyzed the date; Li Song, Wei Xia, and Yaya Feng contributed analysis tools and reagents.

Conflicts of Interest: The authors declare no conflict of interest.

References

1. Porter, N.; Wu, H.; Quan, Z.; Fang, J. Shape-controlled and electrocatalytic activity-enhancement of Pt-based bimetallic nanocrystals. *Acc. Chem. Res.* **2013**, *46*, 1867–1877. [CrossRef] [PubMed]
2. Wang, L.; Yamauchi, Y. Metallic Nanocages: Synthesis of bimetallic Pt–Pd hollow nanoparticles with dendritic shells by selective chemical etching. *J. Am. Chem. Soc.* **2013**, *135*, 16762–16765. [CrossRef] [PubMed]
3. Gasteiger, H.; Markovic, N. Just a dream—Or future reality? *Science* **2009**, *324*, 48–49. [CrossRef] [PubMed]
4. Debe, M. Electrocatalyst approaches and challenges for automotive fuel cells. *Nature* **2012**, *486*, 43–51. [CrossRef] [PubMed]
5. Bashyam, R.; Zelenay, P. A class of non-precious metal composite catalysts for fuel cells. *Nature* **2006**, *443*, 63–66. [CrossRef] [PubMed]
6. Lefevre, M.; Proietti, E.; Jaouen, F.; Dodelet, J. Iron-based catalysts with improved oxygen reduction activity in polymer electrolyte fuel cells. *Science* **2009**, *324*, 71–74. [CrossRef] [PubMed]
7. Liang, Y.; Wang, H.; Zhou, J.; Li, Y.; Wang, J.; Regier, T.; Dai, H. Covalent hybrid of spinel manganese—Cobalt oxide and graphene as advanced oxygen reduction electrocatalysts. *J. Am. Chem. Soc.* **2012**, *134*, 3517–3523. [CrossRef] [PubMed]
8. Ye, Y.; Kuai, L.; Geng, B. A template-free route to a Fe_3O_4-Co_3O_4 yolk-shell nanostructure as a noble-metal free electrocatalyst for ORR in alkaline media. *J. Mater. Chem.* **2012**, *22*, 19132–19138. [CrossRef]
9. Liang, Y.; Li, Y.; Wang, H.; Dai, H. Strongly coupled inorganic/nanocarbon hybrid materials for advanced electrocatalysis. *J. Am. Chem. Soc.* **2013**, *135*, 2013–2036. [CrossRef] [PubMed]
10. Mao, S.; Wei, Z.H.; Huang, T.; You, Y.; Chen, J. High-performance bi-functional electrocatalysts of 3D crumpled grapheme-cobalt oxide nanohybrids for oxygen reduction and evolution reactions. *Energy Environ. Sci.* **2014**, *7*, 609–616. [CrossRef]
11. Xue, H.; Wu, S.; Tang, J.; Gong, H.; He, P.; He, J.; Zhou, H. Hierarchical Porous Nickel Cobaltate Nanoneedle Arrays as Flexible Carbon-Protected Cathodes for High-Performance Lithium–Oxygen Batteries. *ACS Appl. Mater. Interfaces* **2016**, *8*, 8427–8435. [CrossRef] [PubMed]
12. Gong, H.; Xue, H.; Wang, T.; Guo, H.; Fan, X.; Song, L.; Xia, W.; He, J. High-loading nickel cobaltate nanoparticles anchored on three-dimensional n-doped graphene as an efficient bifunctional catalyst for lithium-oxygen batteries. *ACS Appl. Mater. Interfaces* **2016**, *8*, 18060–18068. [CrossRef] [PubMed]
13. Liang, Y.; Li, Y.; Wang, H.; Zhou, J.; Wang, J.; Regier, T.; Dai, H. Co_3O_4 nanocrystals on graphene as a synergistic catalyst for oxygen reduction reaction. *Nat. Mater.* **2011**, *10*, 780–786. [CrossRef] [PubMed]
14. Liang, Y.; Wang, H.; Diao, P.; Chang, W.; Hong, G.; Li, Y.; Gong, M.; Xie, L.; Zhou, J.; Wang, J.; et al. Oxygen reduction electrocatalyst based on strongly coupled cobalt oxide nanocrystals and carbon nanotubes. *J. Am. Chem. Soc.* **2012**, *134*, 15849–15857. [CrossRef] [PubMed]

15. Niu, H.; Zhang, J.; Xie, Z.; Wang, X.; Lin, T. Preparation, structure and supercapacitance of bonded carbon nanofiber electrode materials. *Carbon* **2011**, *49*, 2380–2388. [CrossRef]
16. Gong, K.; Chakrabarti, S.; Dai, L. Electrochemistry at carbon nanotube electrodes: Is the nanotube tip more active than the sidewall? *Angew. Chem. Int. Ed.* **2008**, *47*, 5446–5450. [CrossRef] [PubMed]
17. Xue, H.; Mu, X.; Tang, J.; Fan, X.; Gong, H.; Wang, T.; He, J.; Yamauchi, Y. A nickel cobaltate nanoparticle-decorated hierarchical porous N-doped carbon nanofiber film as a binder-free self-supported cathode for nonaqueous Li–O_2 batteries. *J. Mater. Chem. A* **2016**, *4*, 9106–9112. [CrossRef]
18. Rats, D.; Vandenbulcke, L.; Herbin, R.; Benoit, R.; Erre, R.; Serin, V.; Sevely, J. Characterization of diamond films deposited on titanium and its alloys. *Thin Solid Films* **1995**, *270*, 177–183. [CrossRef]
19. Coutures, J.; Erre, R.; Massiot, D.; Landron, C.; Billard, D.; Peraudeau, G. Ar^+ ion beam effects on M_xO_y-alumina silica glasses. *Radiat. Eff.* **1986**, *98*, 83–91. [CrossRef]
20. Xue, H.; Zhao, J.; Tang, J.; Gong, H.; He, P.; Zhou, H.; Yamauchi, Y.; He, J. High-loading nano-SnO_2 encapsulated in situ in three-dimensional rigid porous carbon for superior lithium-ion batteries. *Chem. Eur. J.* **2016**, *22*, 4915–4923. [CrossRef] [PubMed]
21. Xue, H.; Wang, T.; Zhao, J.; Gong, H.; Tang, J.; Guo, H.; Fan, X.; He, J. Constructing a multicomponent ordered mesoporous carbon for improved electrochemical performance induced by in-situ doping phosphorus. *Carbon* **2016**, *104*, 10–19. [CrossRef]
22. Cui, B.; Lin, H.; Liu, Y.; Li, J.; Sun, P.; Zhao, X.; Liu, C. Photophysical and photocatalytic properties of core-ring structured $NiCo_2O_4$ nanoplatelets. *J. Phys. Chem. C* **2009**, *113*, 14083–14087. [CrossRef]
23. Yuan, C.; Li, J.; Hou, L.; Zhang, X.; Shen, L.; Lou, X. Ultrathin mesoporous $NiCo_2O_4$ nanosheets supported on ni foam as advanced electrodes for supercapacitors. *Adv. Funct. Mater.* **2012**, *22*, 4592–4597. [CrossRef]
24. Tang, J.; Wang, T.; Pan, X.; Sun, X.; Fan, X.; Guo, Y.; Xue, H.; He, J. Synthesis and Electrochemical Characterization of N-Doped Partially Graphitized Ordered Mesoporous Carbon–Co Composite. *J. Phys. Chem. C* **2013**, *3*, 16896–16906. [CrossRef]
25. Tang, J.; Liu, J.; Li, C.; Li, Y.; Tade, M.; Dai, S.; Yamauchi, Y. Synthesis of Nitrogen-Doped Mesoporous Carbon Spheres with Extra-Large Pores through Assembly of Diblock Copolymer Micelles. *Angew. Chem. Int. Ed.* **2015**, *54*, 588–593. [CrossRef]
26. Xue, H.; Tang, J.; Gong, H.; Guo, H.; Fan, X.; Wang, T.; He, J.; Yamauchi, Y. Fabrication of PdCo bimetallic nanoparticles anchored on three-dimensional ordered n-doped porous carbon as an efficient catalyst for oxygen reduction reaction. *ACS Appl. Mater. Interfaces* **2016**, *8*, 20766–20771. [CrossRef] [PubMed]
27. Song, L.; Wang, T.; Ma, Y.; Xue, H.; Guo, H.; Fan, X.; Xia, W.; Gong, H.; He, J. Functional species encapsulated in nitrogen-doped porous carbon as a highly efficient catalyst for the oxygen reduction reaction. *Chem. Eur. J.* **2017**, *23*, 3398–3405. [CrossRef] [PubMed]
28. Song, L.; Wang, T.; Wang, Y.; Xue, H.; Fan, X.; Guo, H.; Xia, W.; Gong, H.; He, J. Porous iron-tungsten carbide electrocatalyst with high activity and stability toward oxygen reduction reaction: From the self-assisted synthetic mechanism to its active-species probing. *ACS Appl. Mater. Interfaces* **2017**, *9*, 3713–3722. [CrossRef] [PubMed]